Hot Adatom Diffusion Following Oxygen Dissociation on Pd(100) and Pd(111): A First-Principles Study of the Equilibration Dynamics of Exothermic Surface Reactions

Vanessa J. Bukas* and Karsten Reuter
Chair for Theoretical Chemistry and Catalysis Research Center, Technische Universität München, Lichtenbergstraße 4, D-85747 Garching, Germany
(Received 30 March 2016; published 28 September 2016)

We augment *ab initio* molecular dynamics simulations with a quantitative account of phononic dissipation to study the hyperthermal adsorbate dynamics resulting from a noninstantaneous energy dissipation during exothermic surface chemical reactions. Comparing the hot adatom diffusion ensuing O_2 dissociation over Pd(100) and Pd(111) we find experimentally accessible product end distances to form a rather misleading measure for the lifetime of this hyperthermal state. The lifetime is particularly long at Pd(111) where a random-walk-type diffusion leads only to small net displacements. A detailed phonon analysis rationalizes the slow equilibration through long-lived Rayleigh mode excitations that spatially confine the released energy within a nanoscopic "hot spot" around the impingement region.

DOI: 10.1103/PhysRevLett.117.146101

There is a long-standing notion that exothermic surface reactions may result in products that are not instantaneously thermalized and thus exhibit a high transient mobility. The prospect of such species acting as "hot" precursors in subsequent reaction steps can strongly influence rates, e.g., in heterogeneous catalysis [1], while their excessive mobility has also been suggested to play a vital role in epitaxial growth mechanisms at low temperatures [2]. Concepts embracing such "hot reactions" have become increasingly established over the past decades [3], yet stimulate groundbreaking implications for prevalent assumptions still fundamentally relied upon in models of chemical kinetics [4]. Assuming instantaneous equilibration at a constant global temperature results, for example, in the Markovian state-to-state hopping that underlies all present-day microkinetic formulations in surface catalysis [5,6].

In the case of dissociative adsorption events, the actual adsorption and any subsequent diffusion of the dissociated products are thereby treated as decoupled, statistically unrelated thermal processes. This presumption is challenged by persistent experimental reports of hyperthermal diffusion or so-called "hot-adatom motion" ensuing the (exothermic) dissociative oxygen adsorption at metal surfaces [7–13]. Corresponding scanning tunneling microscopy studies rely on well-defined single crystal surfaces and controlled dosage in ultrahigh vacuum to produce highest quality data. Working at temperatures that are sufficiently low to suppress thermal diffusion, the transient motion is then inferred from recorded separation distances of adatom pairs in the low-coverage regime.

Even though not undisputed [14], the by far largest separations reported this way are more than 14 surface lattice constants (SLCs) in the case of dissociative O_2 adsorption at Al(111) [7]. While this may be rationalized with the exceptionally large exothermicity of this reaction, other factors like substrate symmetry must also play a role for the dissipation mechanism. Otherwise it is difficult to reconcile the 7–14 SLC separations found for O_2 at Ag(100) [11–13] with the small O-O separations peaking at two SLCs that have been recorded on more reactive Pt-group (111) transition metal surfaces [8,10].

Unable to explicitly access the picosecond dynamical motion, these experiments have unfortunately so far not allowed for any deeper mechanistic analysis or an extraction of the lifetime of the hyperthermal state. The recent development of the QM/Me (quantum mechanics/metal) embedding scheme instead offers this possibility from the perspective of predictive-quality first-principles simulations [15]. This scheme augments a density-functional theory (DFT) based quantum mechanical description of the immediate reaction zone with a quantitative treatment of phononic dissipation into an extended classical heat bath and thus allows to directly follow the dissipation dynamics through *ab initio* molecular dynamics (AIMD) simulations. In a first application to oxygen dissociation over Pd(100) QM/Me indeed predicted a nonimmediate energy transfer to the substrate with the resulting hot O adatoms traveling ballistically over four SLCs [15].

Here, we specifically analyze the role of substrate symmetry and compare this to O_2 dissociation over Pd(111), where previous experiments found hot-adatom motion leading only to shorter O-O separations around $\sqrt{3}$ or 2 times the surface lattice constant [10]. Fully reproducing these experimental end distances, our QM/Me-AIMD simulations intriguingly reveal a much slower equilibration on Pd(111); i.e., the O adatoms on Pd(111) remain hot for a much longer time than on Pd(100). The shorter end distances result instead from the (111) substrate symmetry, which only allows for a random-walk-type diffusion as compared to the directed motion along the

surface channels of the Pd(100) surface. A detailed phonon analysis furthermore relates the slower equilibration dynamics to the random-walk induced excitation of long-lived low-energy surface phonon modes that prevents an efficient dissipation of the reaction energy into the substrate bulk. Hitherto monitored O-O end distances are thus a rather misleading measure of the lifetime of the hyperthermal state.

The QM/Me embedding scheme effectively separates long-range elastic contributions due to displaced substrate atoms from the adsorbate-induced chemical interactions [15]. The latter are then sufficiently short ranged to be captured in periodic-boundary DFT supercell calculations, treating electronic exchange and correlation (xc) at the level of the semilocal Perdew-Burke-Ernzerhof (PBE) functional [16]. As shown in Fig. 1, these supercells contain three layer slabs with a (9×3) and (6×6) surface unit cell for Pd(100) and Pd(111), respectively. The long-range lattice deformation that occurs with the progressing chemical reaction as well as the concomitant phononic dissipation are in turn accounted for through a cubic bath of 125,000 Pd atoms described at the level of the modified embedded atom method (MEAM) [17]. This large bath size provides a quantitative description of the phononic band structure and ensures that phonon propagation has not yet reached the bath boundaries even for the longer AIMD trajectories (3 ps) considered in this work. The QM/Me-AIMD simulations are carried out within the Atomic Simulation Environment (ASE) [18] by loosely interfacing the `FHI-aims` all-electron DFT code [19] and the `LAMMPS` [20] implementation of the MEAM potential. At the employed computational settings, cf., Supplemental Material (SM) [21], and a time step of $\Delta t = 2.5$ fs, a high-quality molecular dynamics energy conservation within 0.5 meV per atom reflects a numerically well-defined Hamiltonian with negligible embedding-induced errors.

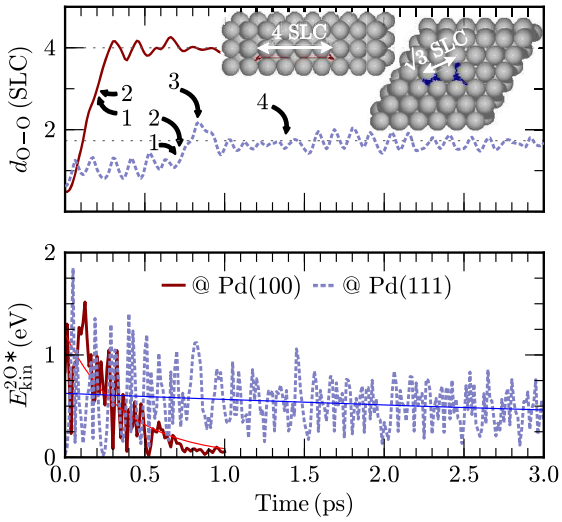

FIG. 1. Dynamical information extracted from QM/Me-AIMD trajectories for O_2 dissociating on Pd(100) (solid) and Pd(111) (dashed lines). Top panel: O-O separation distances in units of the surface lattice constant (SLC ~ 2.79 Å). Hyperthermal adatom hops between neighboring hollow sites are numbered and schematically represented in a top view of the DFT-described reaction zones in the figure's insets (movies of the trajectories are available electronically in Ref. [21]). Lower panel: Oxygen kinetic energies E_{kin}^{2O*} demonstrating the picosecond time scale of energy transfer to the Pd(100) and Pd(111) phononic systems. Note the significantly different decay rates on the two surfaces as estimated from an exponential fit of the data (thin lines).

At Pd(100) a direct dissociation mechanism via one dominant entrance channel [26] provides suitable initial conditions of particular statistical relevance for the QM/Me-AIMD trajectory shown in Fig. 1. This channel steers the impinging O_2 molecule to dissociate side on and with its molecular axis centered above a fourfold hollow site [15]. To initialize trajectories in the precursor-mediated dissociation over Pd(111) [27] we focus instead on the relevant transition states (TS) between molecular and dissociative adsorption as identified via nudged elastic band (NEB) [28] calculations. The trajectory shown in Fig. 1 results specifically from the TS for the dissociation of a molecular precursor in the top-face-centered-cubic(FCC)-bridge configuration, i.e., with the O_2 center of mass essentially above a threefold FCC hollow site and the molecular axis oriented along the $[1\bar{2}1]$ direction. On both surfaces, the O_2 molecule is only given a negligibly small initial kinetic energy, so that both reactions are dominated by the large intrinsic exothermicity of the dissociation event.

Figure 1 illustrates the ensuing equilibration dynamics during both trajectories, where d_{O-O} directly measures the adatom separation distance as a function of time. The decay of the adsorbate kinetic energies presented in the lower panel shows both reactions to give rise to translationally hot products that are not instantaneously thermalized. The resulting transient mobility is marked by a series of hyperthermal diffusive hops between neighboring binding sites that occur on a ps time scale and are indicated by arrows in Fig. 1. Specifically, two such hops yield a largely increasing d_{O-O} on Pd(100) as the adatoms travel along the [001] surface channels and promptly equilibrate over hollow sites at four SLCs (~11.2 Å) apart. A random-walk-type diffusion is instead found on the densely packed Pd(111) surface that has the adatoms primarily trapped in the vicinity of hollow sites. Collisions with neighboring Pd atoms randomize the direction of the O lateral motion so that even the four barrier crossings counted along the presented 3 ps trajectory eventually lead only to the occupation of FCC adsorption sites at a much smaller distance of $\sqrt{3}$ times the SLC (~4.8 Å). Trajectories started at the dissociative TS above FCC or hexagonal-close-packed (HCP) hollow sites (not shown) lead to similarly short end distances (in the range of 1–3 SLCs) of which the most common is two times the SLC, exactly as seen in experiment [10].

The formation of hot adatoms on both surfaces does not come as altogether too surprising given the similarly high exothermicity of the dissociative reactions [2.3 vs 2.7 eV for O_2 on Pd(100) and Pd(111) at DFT-PBE level, respectively] and barriers for atomic diffusion (179 vs 327 meV). Difficult to reconcile on purely energetic grounds, however, is the markedly longer lifetime predicted for this hyperthermal phase on Pd(111). Even after 3 ps Fig. 1 reveals intriguingly hot adsorbates with fluctuations in kinetic energy on the order of 0.5 eV, i.e., an effective temperature amounting to several thousands of kelvin. Similarly long equilibration times are obtained in a total of nine other trajectories starting from the different TSs and slightly varying initial conditions. In all cases we observe a random-type walk with much longer absolute distances traveled than suggested by the small final equilibrium separation. Computed decay constants suggest an average of 10 ps to a full thermalization that is to be contrasted with the much shorter 1.2 ps obtained for the reaction at Pd(100), cf., Fig. 1.

These substantially different equilibration rates on the two surfaces arise from qualitative differences in the phononic response that already set in during the very early stages of the O_2 dissociation dynamics. We directly access this phononic information from the QM/Me-AIMD trajectories through the projection scheme originally laid out by McGaughey and Kaviany [29], yet appropriately extended here for the polyatomic primitive cell of a two-dimensional slab model [30]. In short, backfolding Γ-point phonons into the (original) larger primitive Brillouin zone defines mode-specific expansion coefficients that can in turn be used for evaluating the energy contained within a single harmonic phonon mode. Instantaneous application at any given AIMD time step can thus quantify phononic energy uptake "on the fly" without the need for averaging over time, while the underlying mode selectivity allows us to focus on certain groups of modes. In particular the surface phonons obviously form a very prominent group in this context and are classified here as modes whose displacement eigenvector is localized to at least 20% in the two outermost slab layers.

Figure 2(b) shows a corresponding phonon excitation spectrum calculated at $t = 75$ fs along the O_2/Pd(100) trajectory, i.e., when dissociation is right in progress with the O-O distance having reached about one SLC. Intriguingly, despite their negligible spectral weight illustrated by the also shown phononic DOS, surface modes have taken up more than a third of the total energy that has been dissipated into the substrate at that time. Quite in contrast to what is predominantly assumed about energy sinks in model bath Hamiltonians (cf., for example, Refs. [31–33] and references therein), it is thereby not the low-frequency Rayleigh modes that become dominantly excited, even though they lie energetically below the onset of the bulk part of the spectrum [30]. The energy

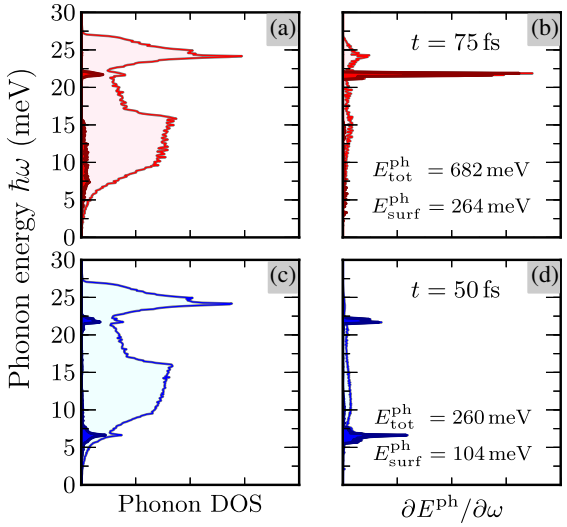

FIG. 2. Rightmost panels: Energy resolved phonon excitation spectra during the early stages of O_2 dissociation on Pd(100) (top) and Pd(111) (bottom). The total amount of phononic energy ($E^{\rm ph}_{\rm tot}$) along with the fraction assigned to surface modes ($E^{\rm ph}_{\rm surf}$) are noted. Leftmost panels: The corresponding Pd equilibrium DOS calculated for 40-layer slabs are shown for reference. In all cases the contribution of localized surface modes is indicated by thick blue/red lines.

is instead highly concentrated in a surface optical phonon band, which lies in a pseudogap of bulk modes at frequencies of 21–23 meV as shown in the SM. Analyzing the mode eigenvectors, this unexpected result can be rationalized by the preferred binding site of the O adatoms. Rather than indenting the topmost substrate layer upon impingement, which is the picture suggesting a predominant excitation of corresponding Rayleigh modes, the dissociating O atoms penetrate directly into the hollow sites and subsequently diffuse laterally over bridge sites along one of the [001] surface channels. Along this motion they rather push the top-layer Pd atoms laterally away, which corresponds exactly to the purely longitudinal displacement pattern of the modes belonging to the aforementioned surface optical phonon band.

Figure 2(d) reveals a rather different phonon excitation spectrum upon O_2 dissociation at the Pd(111) surface. Here, the random-walk-type diffusion mechanism rather leads to a weighted phonon population that essentially follows the surface DOS and has the larger fraction of the released chemical energy contained within low-frequency acoustic phonons. Behold some quantitative variations; this characteristic excitation of notoriously long-lived Rayleigh waves [34] at short wavelengths, cf., insets in Fig. 3, is consistently obtained for all QM/Me-AIMD trajectories starting from the different dissociative TSs. With their small group velocities, cf., SM, these modes efficiently confine the released energy within a small reaction zone around the impingement region. As reflected by the nonmonotonic behavior in the total phononic energy uptake, cf., SM, this

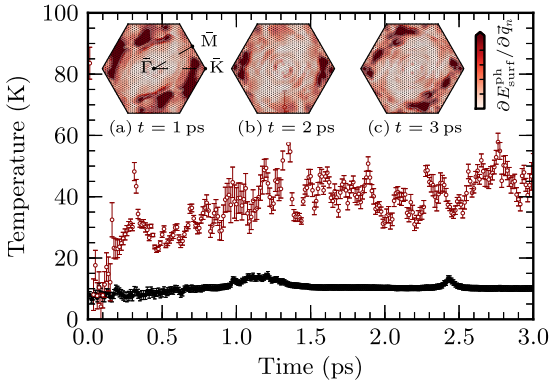

FIG. 3. Time-dependent temperature profiles for the Pd(111) surface hot spot (open) and bulk thermal bath (closed markers) as extracted from respective Planckian distributions at every QM/Me-AIMD time step (standard errors indicate the fit quality). Insets (a)–(c): Distribution of surface phonon energy (E^{ph}_{surf}) over the two-dimensional surface Brillouin zone at the noted times. The coloring is based on a linear interpolation between values at exact phonon wave vectors ($\vec{q}_n$, black markers) at which the energy of all phonon branches has been summed.

promotes a back and forth energy exchange between the O adatoms and the surface Pd atoms. In contrast, the (sub-ps) anharmonic decay of the highly populated surface optical modes at Pd(100) quickly dissipates the energy at a constant rate of ~ 2 meV/fs into the bulk at a concomitant much shorter lifetime of the hyperthermal state.

The situation at Pd(111) carries thus all characteristics of a phonon hot spot [35], in which the energy released into the phononic system stays confined in a nanoscopic region. After 3 ps we indeed find about one half of the system's total kinetic energy to still be within the confines of the DFT supercell, i.e., in the immediate reaction zone. Within this region phonon-phonon coupling quickly establishes a quasiequilibrium phonon distribution that is sufficiently well described by a Planckian distribution. This allows us to assign a local phonon temperature that we contrast in Fig. 3 to a similarly assigned phonon temperature of the Pd bulk modes. These results confirm a minimal coupling of the two subsystems over the entire course of the QM/Me-AIMD trajectory, with the surface hot spot eventually reaching an effective temperature that is five times larger than its bulk counterpart and still rising. The small extent of the hot spot leads thereby to an enormous effective energy density of the order of 2.7 eV/10 $nm^3 \sim 10$ J/cm^3 created by a singular molecular event. Even though modern high-fluency laser pulses reach even higher absorbed energy densities than this [36], much of this energy is there primarily deposited into electron-hole (e-h) pairs, which efficiently dissipate this energy over a larger volume. At present, our electronically adiabatic theory does not account for this dissipation channel at all. However, we do not expect this channel to be large. Using the calculated average velocity of all Pd atoms in the QM reaction zone over the course of the QM/Me-AIMD trajectory to evaluate the accumulated loss due to electronic friction [37], we arrive at a rough estimate of only 22 meV after 3 ps. This suggests that the "hot chemistry" ensuing the exothermic surface reaction is qualitatively different to laser-driven photochemistry, where particularly for chemisorbed adsorbates the excitation of hot electrons is generally believed to play a crucial role [41].

Similarities might instead be higher for radiation damage aspects like the transient recoil of nuclei under neutron bombardment. The presented QM/Me methodology is generally suitable for application to any problem that breaks a metal's translational symmetry in any number of periodic directions. Beyond its relevance within the surface science context (for instance to address adsorbate-induced reconstructions), it may therefore readily be employed to follow bulk diffusion or address the chemistry around bulk defects and dislocations [42].

In conclusion, we have studied the equilibration dynamics ensuing the exothermic O_2 dissociation at Pd(100) and Pd(111). The obtained *ab initio* molecular dynamics results indicate that hitherto considered product end distances provide a misleading measure of the transient hot adatom mobility that results from a noninstantaneous dissipation of the released energy. The lifetime of this hyperthermal state might be particularly long precisely in situations where the substrate symmetry or higher surface coverages enforce a random-walk-type diffusion. While leading to small net displacements, this type of diffusion favors the excitation of long-lived Rayleigh surface phonon modes, which efficiently confine the released chemical energy within a nanoscopic hot spot around the impingement region. This suggests that transient mobility might be more common than hitherto anticipated, possibly extending particularly to systems where it has been dismissed on the basis of nearest-neighbor-type end distances. From the computed decay constants, we estimate an average of 10 ps to a full thermalization of the O adatoms at Pd(111). With an initial kinetic energy corresponding to several thousands of kelvin this is a long time to induce hot chemistry.

S. P. Rittmeyer is thanked for the nonadiabatic energy loss estimate and for many stimulating discussions. Funding through the Deutsche Forschungsgemeinschaft is acknowledged within Grant No. RE1509/19-1, as is generous access to CPU time through the Leibniz Rechenzentrum der Bayerischen Akademie der Wissenschaften (Grant No. pr85wa).

*vanessa.bukas@ch.tum.de

[1] J. Harris and B. Kasemo, Surf. Sci. **105**, L281 (1981).
[2] W. F. Egelhoff and I. Jacob, Phys. Rev. Lett. **62**, 921 (1989).
[3] A. Carley, P. Davies, and M. Roberts, Catal. Lett. **80**, 25 (2002).

[4] G. Ertl, in *Impact of Surface Science on Catalysis*, Advances in Catalysis Vol. 45 (Academic Press, New York, 2000), pp. 1–69.

[5] I. Chorkendorff and J. W. Niemantsverdriet, in *Concepts of Modern Catalysis and Kinetics* (Wiley-VCH Verlag GmbH & Co. KGaA, Weinheim, Germany, 2005), pp. 267–299.

[6] K. Reuter, in *Modeling and Simulation of Heterogeneous Catalytic Reactions* (Wiley-VCH Verlag GmbH & Co. KGaA, Weinheim, Germany, 2011), pp. 71–111.

[7] H. Brune, J. Wintterlin, R. J. Behm, and G. Ertl, Phys. Rev. Lett. **68**, 624 (1992).

[8] J. Wintterlin, R. Schuster, and G. Ertl, Phys. Rev. Lett. **77**, 123 (1996).

[9] B. G. Briner, M. Doering, H.-P. Rust, and A. M. Bradshaw, Phys. Rev. Lett. **78**, 1516 (1997).

[10] M. Rose, A. Borg, J. Dunphy, T. Mitsui, D. Ogletree, and M. Salmeron, Surf. Sci. **561**, 69 (2004).

[11] S. Schintke, S. Messerli, K. Morgenstern, J. Nieminen, and W.-D. Schneider, J. Chem. Phys. **114**, 4206 (2001).

[12] M.-F. Hsieh, D.-S. Lin, H. Gawronski, and K. Morgenstern, J. Chem. Phys. **131**, 174709 (2009).

[13] C. Sprodowski, M. Mehlhorn, and K. Morgenstern, J. Phys. Condens. Matter **22**, 264005 (2010).

[14] M. Schmid, G. Leonardelli, R. Tschelienig, A. Biedermann, and P. Varga, Surf. Sci. **478**, L355 (2001).

[15] J. Meyer and K. Reuter, Angew. Chem., Int. Ed. Engl. **53**, 4721 (2014).

[16] J. P. Perdew, K. Burke, and M. Ernzerhof, Phys. Rev. Lett. **77**, 3865 (1996); **78**, 1396 (1997).

[17] M. I. Baskes, Phys. Rev. B **46**, 2727 (1992).

[18] S. R. Bahn and K. W. Jacobsen, Comput. Sci. Eng. **4**, 56 (2002).

[19] V. Blum, R. Gehrke, F. Hanke, P. Havu, V. Havu, X. Ren, K. Reuter, and M. Scheffler, Comput. Phys. Commun. **180**, 2175 (2009).

[20] S. Plimpton, J. Chem. Phys. **117**, 1 (1995).

[21] See Supplemental Material at http://link.aps.org/supplemental/10.1103/PhysRevLett.117.146101 for a detailed description of the employed computational settings, phonon dispersion, energy uptake, and movies of the presented QM/Me-AIMD trajectories. The Supplemental Material includes the additional Refs. [22–25].

[22] A. Eichler, F. Mittendorfer, and J. Hafner, Phys. Rev. B **62**, 4744 (2000).

[23] C. Carbogno, A. Gross, J. Meyer, and K. Reuter, in *Dynamics of Gas-Surface Interactions*, edited by R. D. Muiño and H. F. Busnengo, Springer Series in Surface Sciences Vol. 50 (Springer, New York, 2013), pp. 389–419.

[24] D.-J. Liu and J. W. Evans, Phys. Rev. B **89**, 205406 (2014).

[25] H. J. Monkhorst and J. D. Pack, Phys. Rev. B **13**, 5188 (1976).

[26] V. J. Bukas, S. Mitra, J. Meyer, and K. Reuter, J. Chem. Phys. **143**, 034705 (2015); V. J. Bukas, J. Meyer, M. Alducin, and K. Reuter, Zeitschrift für Physikalische Chemie **227**, 1523 (2013).

[27] P. Sjövall and P. Uvdal, Chem. Phys. Lett. **282**, 355 (1998); P. Nolan, B. Lutz, P. Tanaka, and C. Mullins, Surf. Sci. **419**, L107 (1998).

[28] G. Henkelman, B. P. Uberuaga, and H. Jónsson, J. Chem. Phys. **113**, 9901 (2000).

[29] A. J. H. McGaughey and M. Kaviany, Phys. Rev. B **69**, 094303 (2004).

[30] J. Meyer, Ph.D. thesis, Freie Universität Berlin, 2012.

[31] M. D. Stiles, J. W. Wilkins, and M. Persson, Phys. Rev. B **34**, 4490 (1986).

[32] M. Hand and J. Harris, J. Chem. Phys. **92**, 7610 (1990).

[33] B. Jackson, Comput. Phys. Commun. **80**, 119 (1994).

[34] S.-I. Tamura, Phys. Rev. B **30**, 610 (1984).

[35] J. C. Hensel and R. C. Dynes, Phys. Rev. Lett. **39**, 969 (1977).

[36] M. Bonn, S. Funk, C. Hess, D. N. Denzler, C. Stampfl, M. Scheffler, M. Wolf, and G. Ertl, Science **285**, 1042 (1999).

[37] The accumulated nonadiabatic energy loss due to electronic friction [38] is estimated as $\eta = \int_0^{\Delta t} dt \eta \langle v \rangle^2(t)$, where $\langle v \rangle^2(t)$ is the average velocity per Pd atom in the reaction zone and $\Delta t = 3$ ps is the length of the QM/Me-AIMD trajectory. The respective electronic friction coefficient η is evaluated for a Pd atom embedded in jellium [39] with an electronic density equal to the Wigner-Seitz radius of bulk Pd [40].

[38] J. I. Juaristi, M. Alducin, R. DiezMuiño, H. F. Busnengo, and A. Salin, Phys. Rev. Lett. **100**, 116102 (2008); S. P. Rittmeyer, J. Meyer, J. I. Juaristi, and K. Reuter, Phys. Rev. Lett. **115**, 046102 (2015).

[39] A. Arnau, P. Echennique, and R. Ritchie, Nucl. Instrum. Methods Phys. Res. **33**, 138 (1988).

[40] V. Moruzzi, J. Janak, and A. Williams, in *Calculated Electronic Properties of Metals*, edited by V. Moruzzi, J. Janak, and A. Williams (Pergamon, New York, 1978), pp. 1–10.

[41] P. Saalfrank, Chem. Rev. **106**, 4116 (2006); I. Lončarić, M. Alducin, P. Saalfrank, and J. I. Juaristi, Phys. Rev. B **93**, 014301 (2016).

[42] S. Dudarev, Annu. Rev. Mater. Res. **43**, 35 (2013).